Absence of hyperfine effects in 13C-graphene spin-valve devices

Wojtaszek, M.; Vera-Marun, I.J.; Whiteway, E.; Hilke, M.; Wees, B.J. van

Published in:
Physical Review B

DOI:
10.1103/PhysRevB.89.035417

Publication date:
2014

Supplementary Information

Absence of hyperfine effects in ^{13}C-graphene spin valve devices.

M. Wojtaszek,[1] I. J. Vera-Marun,[1] E. Whiteway,[2] M. Hilke,[2] and B. J. van Wees[1]

[1]*Physics of Nanodevices, Zernike Institute for Advanced Materials, University of Groningen, Groningen, The Netherlands**

[2]*Department of Physics, McGill University, Montreal, Canada*

PACS numbers: 72.25.-b, 85.75.-d, 31.30.Gs

I. COMPARISON OF SPIN PROPERTIES OF ^{13}C-GRAPHENE AT ROOM TEMPERATURE AND T = 4.2 K.

Hyperfine effects are most pronounced at low temperatures due to less thermal fluctuations of nuclear spin, hence we want to compare the spin transport properties at room temperature versus T = 4.2 K, extracted from Hanle measurements for parallel and antiparallel contacts configuration as a function of gate voltage. The fitting of Hanle precession curves gives independent values for spin relaxation time τ_s and spin diffusion D_s, from which we get $\lambda_s = \sqrt{\tau_s D_s}$. All these coefficients are summarized in Fig. 1. Alternatively, from the charge transport measurements we can determine charge diffusion constant D_c using the Einstein relation $\sigma = e\nu(E)D_c$, where $\nu(E)$ is the density of states of graphene at T = 0 K and $\sigma = 1/\rho$ is its sheet conductivity. The singularity of D_c around $n = 0$ arises due to the vanishing number of states at the Dirac point and can be eliminated by including the broadening of states[1]. Nevertheless, as these corrections are negligible at the large doping, in metallic regime one can rely on D_c determined using the ideal, zero-temperature density of states. We can see that for large n $D_c \simeq D_s$, like in exfoliated graphene[1]. In graphene with intrinsic magnetic fields from defects[2,3], there appears an extra scaling of the precession term $\frac{g\mu_B}{\hbar}\boldsymbol{B}$, because the external magnetic field, used in the fitting procedure, is different from the total magnetic field experienced by spins. Such a scaling can be also seen as a change in the graphene g-factor, $g \to g^*$, and it affects the determination of spin coefficients: $\tau_s = \frac{g^*}{g}\tau_s^*$, $D_s = \frac{g}{g^*}D_s^*$. This similarity between D_s and D_c, determined by two independent methods, implies that there is no change in g-factor due to internal (here nuclear) fields, and the spin coefficients are properly determined. The values for τ_s range from 60 to 100 ps, depending on the doping, and they barely change with the temperature. Similar weak dependence of τ_s on temperature is also present in exfoliated graphene, although τ_s, determined from Hanle precession, is 2-10 times higher[4,5]. The observed lower values of τ_s are also found in the control sample - a CVD graphene from pure ^{12}C precursor and therefore cannot be attributed to the hyperfine effects. A lower τ_s can originate from crystal defects and rippling of graphene sheet, which is inherent to the growth and transfer conditions, the quality of the Cu substrate and eventual remaining of $FeCl_3$ etchant.

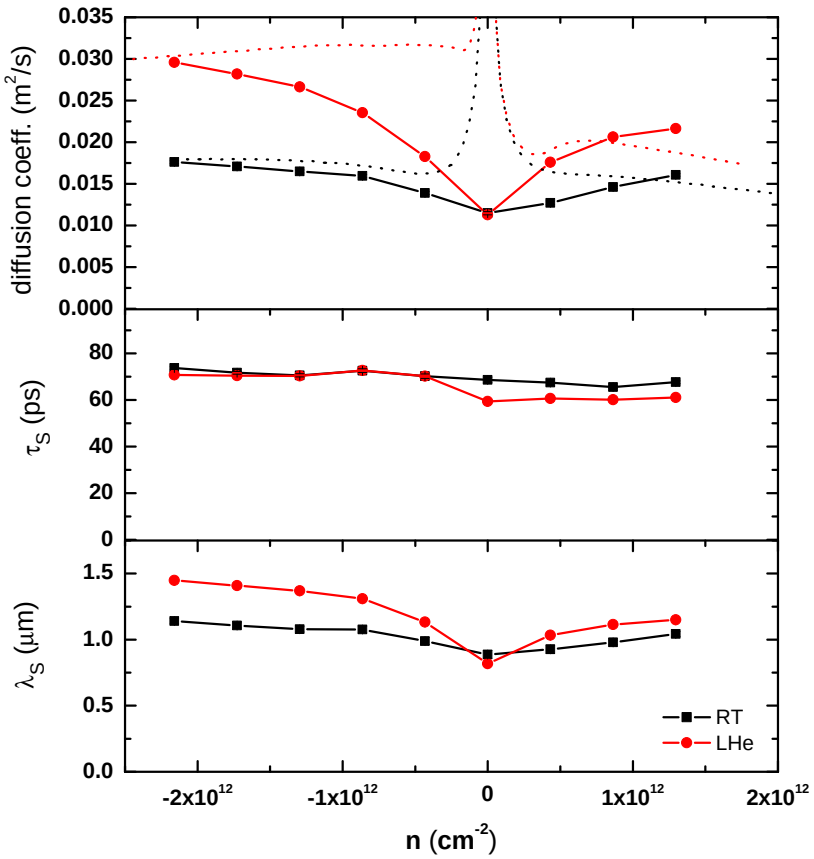

FIG. 1: (Color online) Comparison of transport properties at room temperature and at T = 4.2 K as a function of carrier concentration. Top panel: diffusion coefficient, central panel: spin relaxation time τ_s, bottom panel: spin relaxation length λ_s. Dotted line represents D_c, calculated using the Einstein relation (from charge transport), D_s, τ_s are extracted from the Hanle curves with subtracted background and $\lambda_s = \sqrt{D_s \tau_s}$.

II. SIMULATION OF OBLIQUE EFFECTS IN GAAS.

In standard Hanle precession experiment the magnetic field is set perpendicular to graphene plane $\boldsymbol{B} = (0, 0, B)$, thus the precession term $\boldsymbol{B} \times \boldsymbol{\mu_s}$ of Bloch equation (Eq. 1 in the main text) vanishes in z-direction. Additionally, the magnetization of injecting contact, and in consequence orientation of injected spins, lies in the x-y plane. Therefore, one can simplify the description of spin dynamics by considering the spin accumulation vector only in two-dimensions: $\boldsymbol{\mu_s} = (\mu_{s,x}, \mu_{s,y})$. However, for a general orientation of external magnetic field $\boldsymbol{\mu_s}$ needs to be considered in all 3 directions. To observe the electron spin dephasing from the nuclear field it is necessary to apply an external field at an oblique angle, which

will redirect the nuclear magnetization from its collinear alignment to the electron spin. Additionally, the mutual dependence of hyperfine field $\boldsymbol{B_n}$ and spin accumulation $\boldsymbol{\mu_s}$ (Eq. 3 in the main text) leads to a non-linear term in Bloch equation, and requires self-consistent solving. These two aspects: a need for a general 3D form of Bloch equation and non-linear dependence of μ_s make the predictions of the spin signal very difficult. To tackle this problem we use a finite-element software package (COMSOL Multiphysics, version 4.3) which allows to define a set of partial differential equations (PDE) and solve it for an user defined geometry. We use a two channel model[6] for spin transport, in which we define spin-dependent chemical potential as a variable ($\boldsymbol{\mu_\uparrow}$, $\boldsymbol{\mu_\downarrow}$), where $\boldsymbol{\mu_s} = \boldsymbol{\mu_\uparrow} - \boldsymbol{\mu_\downarrow}$. In arbitrary external magnetic fields, not necessary perpendicular to the graphene plane, the electron spins change their orientation, therefore we define the chemical potential in 3D spin space separately for each spin channels: $\boldsymbol{\mu_{\uparrow/\downarrow}} = (\mu_x^{\uparrow/\downarrow}, \mu_y^{\uparrow/\downarrow}, \mu_z^{\uparrow/\downarrow})$. The up and down arrows refer to the spin orientation only at the point of injection and not at the distances further away from injector, where spin orientation undergoes precession. We emulate the spin dynamics separately for each spin channel, linking them only by spin relaxation. In this problem the charge and spin transport are coupled, therefore when solving the diffusion equation the conservation of generalized currents $\nabla(\boldsymbol{J_\uparrow}, \boldsymbol{J_\downarrow}) = f(\boldsymbol{\mu_\uparrow}, \boldsymbol{\mu_\downarrow})$ has to be satisfied. The conservation of charge current is given by $\nabla(\sigma_\uparrow \nabla \boldsymbol{\mu_\uparrow} + \sigma_\uparrow \nabla \boldsymbol{\mu_\downarrow}) = 0$. In non-magnet $\sigma_\uparrow = \sigma_\downarrow$, while in ferromagnet $\sigma_\uparrow = (1+P)(\sigma_\uparrow + \sigma_\downarrow)$, $\sigma_\downarrow = (1-P)(\sigma_\uparrow + \sigma_\downarrow)$, where P is a polarization of a ferromagnetic contact. The conservation of spin is derived from Valet-Fert equation with additional precession term $\nabla^2 \boldsymbol{\mu_s} = \boldsymbol{\mu_s}/\lambda^2 - \boldsymbol{\omega} \times \boldsymbol{\mu_s}/D_s$, where the term $\boldsymbol{\omega} = \frac{g\mu_B}{\hbar}(\boldsymbol{B} + \boldsymbol{B_n})$ includes external and nuclear magnetic field. The 3D COMSOL model includes full geometry of the device together with ferromagnetic contacts and the tunnel barriers of finite resistance.

To verify our model we choose GaAs system and spin transport results of Chan *et al.*[7] as a reference. We set the device geometry corresponding to the one reported (meshed with tetrahedrons) and set charge and spin transport coefficients from the values determined therein: b_n = -5.3 T, b_e = -5 mT, τ_s = 10 ns, λ_s = 5 μm, L = 10 μm, GaAs polarization $\beta_{GaAs} = \frac{3\mu_s}{E_F}$, where $E_F \simeq 7.5$ meV, $P = 0.2$.

We first emulate the lineshape of the GaAs spin valve signal in presence of small, fixed, out-of-plane field component B_z = 2 mT as a function of polarizing current I_{DC}, see Fig. 2a. For parallel contact magnetization (↑↑) we observe a formation of the depolarization dip around B_x=0, of which amplitude increases with electron spin accumulation. A plot of the

expected signal in the absence of nuclear polarization ($b_n = 0$, dashed line) shows a broad, single dip, corresponding to the inverted Hanle effect due to the presence of small constant out-of-plane field component B_z. The structure of the hyperfine dips mirrors along $B = 0$ axis when the polarization of contacts reverses (from $\uparrow\uparrow$ to $\downarrow\downarrow$), see inset in Fig. 2a. This is directly related to the change in the vectorial configuration of the magnetic fields involved and was also confirmed experimentally[7].

Next we simulate the oblique Hanle effect by setting an external field at oblique angle $\theta = 10^o$, so $\boldsymbol{B} = (B\sin\theta, 0, B\cos\theta)$. With an increase of I_{dc} a central Hanle peak shifts to the positive field values, creating an asymmetric lineshape, see Fig 2b. Additionally, the maximum peak at B=0 splits into two, see inset in Fig 2b. This complex lineshape is a result of subtle interplay between all the magnetic fields included in the problem. These features are less pronounced than the dips in the spin-valve signal and require much higher spin accumulation to be resolved.

All the obtained features are in agreement with the experimental findings of Chan *et al.*[7], confirming the validity of our model.

III. BUILDING UP NUCLEAR POLARIZATION - MINOR LOOP SCAN.

As motivated in the main text the correlation time between delocalized conducting electrons and nuclei is very short and requires times of the order $\sim 10^4$ s to build up dynamical nuclear polarization. For that reason we perform a spin-valve measurement in a reduced magnetic field range, such that only the detector contact switches its magnetization (so called minor loop measurement). This way the injected polarizing current $I_{dc} = 30\mu$A has always the same spin direction. The eventual formation of dephasing dips in R_{nl} around zero field is monitored as a function of time by performing continuous field sweeps. We measure the effect at the closest distance between injector-detector, where the spin accumulation is the highest. We perform 50 sweeps within the total time of 250 minutes ($\simeq 1.5 \cdot 10^4$ s), the first and the last sweep can be seen in Fig. 3. The scans are identical except for the shift in common background. No extra dips around B=0, which could be attributed to polarized nuclei can be resolved.

This, as well as other measurements reported here, confirms the negligible role of hyperfine interactions between electrons and nuclei in graphene.

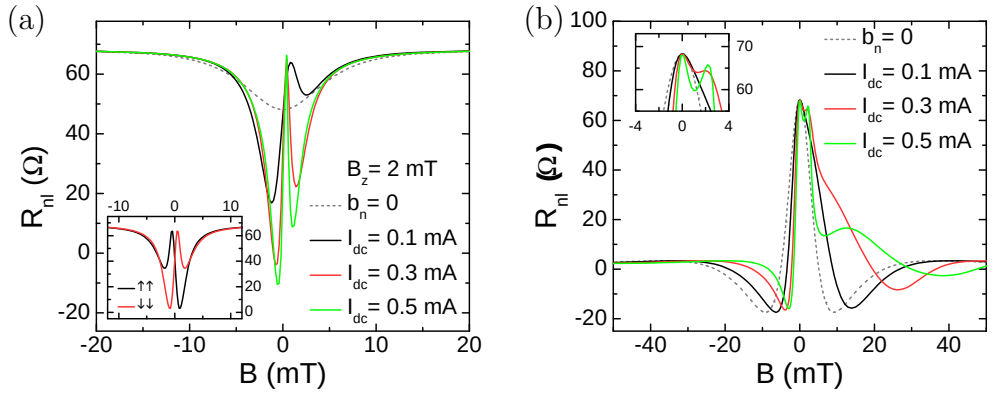

FIG. 2: (Color online) (a) Simulated oblique non-local spin signal in presence of hyperfine field in GaAs for different values of polarizing current I_{dc}. The increase of polarization translates to increase of depolarization dips around $B = 0$. The dashed line presents the signal in case of no hyperfine interactions ($b_n = 0$). The inset shows mirroring property of the spin signal in parallel contact configuration between different magnetization directions (↑↑ or ↓↓). b) Simulated oblique Hanle precession signal for $\theta = 10^o$. With the increase of polarization I_{dc} the central Hanle peak shifts it position and an asymmetry builds up. The inset zooms at the $B = 0$, where the central peak splits.

IV. NMR STUDIES OF THE GRAPHENE TRANSPORT.

As a last check of the possible correlation between nuclear field and spin dephasing mechanisms we try to induce nuclear magnetic resonance in ^{13}C nuclei. Upon the high frequency electromagnetic field, which energy matches the energy difference between the nuclear spin levels, we can induce transitions between these states, thus enhancing the randomization of the nuclear field. This causes the change in the effective magnetic field acting on electron spins from polarized nuclei, which could affect the spin signal provided that the nuclear polarization and hyperfine interactions are sufficiently strong. The resonance frequency for ^{13}C nuclei appears at 10.7 MHz/T [8]. To investigate this effect we fabricated a device with a waveguide in its close vicinity to exert an RF modulation of nuclear magnetic moment. Then, at $T = 4.2$ K, we measure the non-local spin-valve signal $V_{nl}^{\uparrow\uparrow}$ as a function of RF frequency f, when crossing the resonance. We set $\boldsymbol{B}$= 0.22 T, which corresponds to a resonance frequency $\nu_{^{13}C} = 2.355$ MHz. We set the field at the oblique angle θ=10° and inject a large polarizing current $I_{dc} = 50$ μA together with a small ac component ($I_{ac} = 1$ μA)

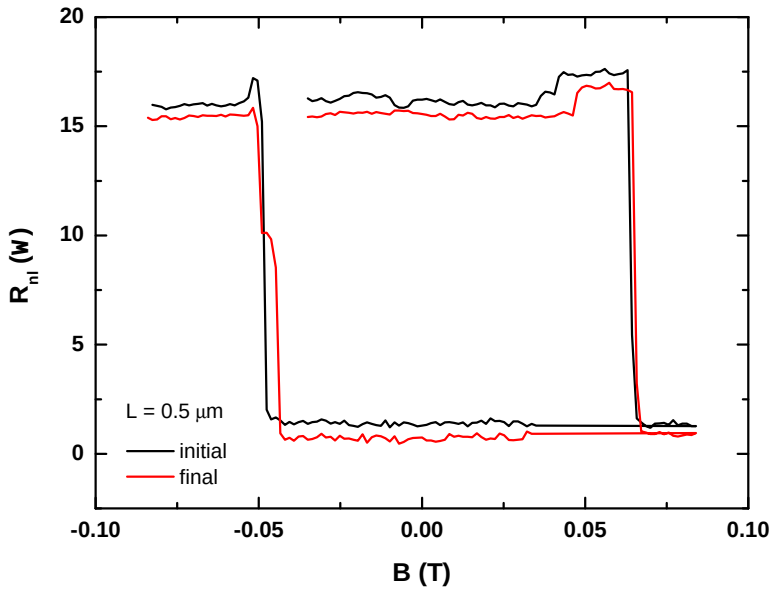

FIG. 3: (Color online) First and last (50^{th}) measurement of minor loop from a set of 50 consecutive scans. The distance between injector and detector L = 0.5 μm, the polarizing current $I_{dc} = 30$ μA, at T = 4.2 K.

for lock-in detection ($L = 1\mu$m). This way we enhance the possible nuclear polarization so that its randomization under resonance conditions could be detected. If the polarized nuclei induce spins dephasing, then upon NMR and the decrease of nuclear polarization the electron spin signal should increase. We apply the RF field of 5 dBm power and vary it with a step of 1 kHz (the RF field $B_{RF} \lesssim 1$ mT). The obtained curve, see Fig. 4, shows no apparent features when sweeping across the resonance frequency, indicated by dashed line. This supports again the observation of negligible influence of nuclear magnetic moment for spin dephasing in graphene.

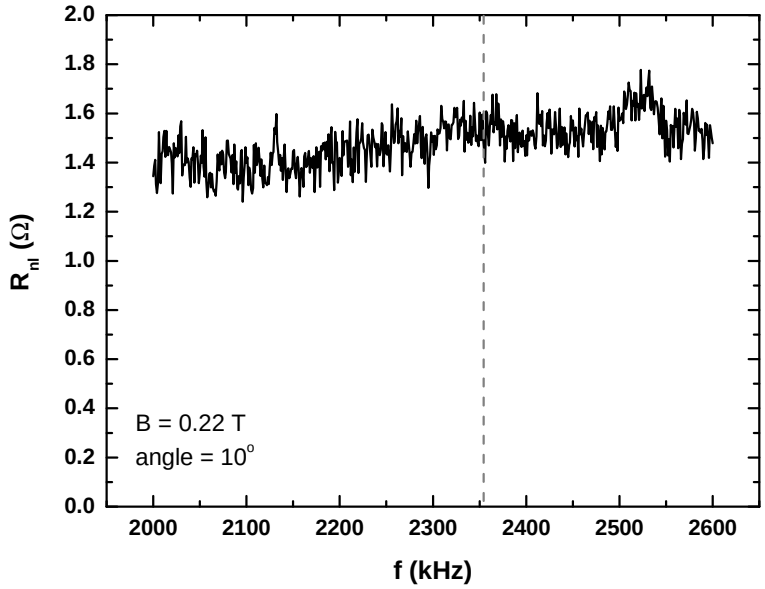

FIG. 4: (Color online) A non-local resistance as a function of applied RF frequency for parallel contacts magnetization at T = 4.2 K and $\boldsymbol{B}$= 0.22 T at oblique angle θ= 10°. In this configuration we expect a resonance (and increase of R_{nl}) at $\nu_{^{13}C}$ = 2.355 MHz, indicated by the dashed line, however, no resonance peak could be distinguished. The frequency step is 1 kHz.

* Electronic address: m.wojtaszek@rug.nl

[1] C. Józsa, T. Maassen, M. Popinciuc, P. J. Zomer, A. Veligura, H. T. Jonkman, and B. J. van Wees, Phys. Rev. B **80**, 241403 (2009).

[2] K. M. McCreary, A. G. Swartz, W. Han, J. Fabian, and R. K. Kawakami, Phys. Rev. Lett. **109**, 186604 (2012).

[3] B. Birkner, D. Pachniowski, A. Sandner, M. Ostler, T. Seyller, J. Fabian, M. Ciorga, D. Weiss, and J. Eroms, Phys. Rev. B **87**, 081405 (2013).

[4] N. Tombros, C. Józsa, M. Popinciuc, H. T. Jonkman, and B. J. van Wees, Nature **448**, 571 (2007).

[5] W. Han and R. K. Kawakami, Phys. Rev. Lett. **107**, 047207 (2011).

[6] T. Valet and A. Fert, Phys. Rev. B **48**, 7099 (1993).

[7] M. Chan, Q. Hu, J. Zhang, T. Kondo, C. Palmstrøm, and P. Crowell, Phys. Rev. B **80**, 161206 (2009).

[8] R. K. Harris and B. E. Mann, *NMR and the Periodic Table* (1978).